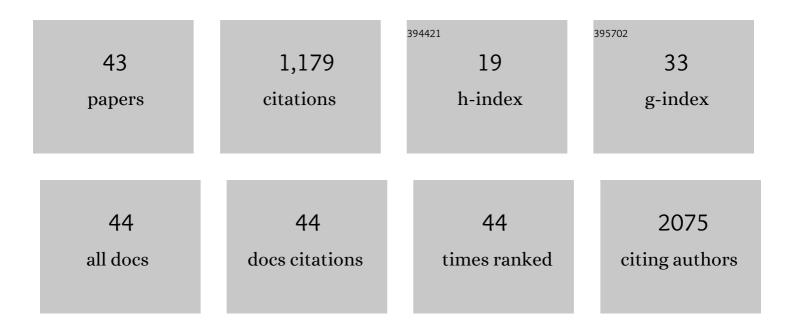
Linda Chaabane

List of Publications by Year in descending order

Source: https://exaly.com/author-pdf/8513665/publications.pdf Version: 2024-02-01



#	Article	IF	CITATIONS
1	Fingolimod may support neuroprotection via blockade of astrocyte nitric oxide. Annals of Neurology, 2014, 76, 325-337.	5.3	142
2	Detrimental and protective action of microglial extracellular vesicles on myelin lesions: astrocyte involvement in remyelination failure. Acta Neuropathologica, 2019, 138, 987-1012.	7.7	120
3	Atherosclerotic Plaques: Classification and Characterization with T2-weighted High-Spatial-Resolution MR Imaging—An in Vitro Study. Radiology, 2001, 219, 403-410.	7.3	103
4	Dose-Related Effects of Repeated ETC-216 (Recombinant Apolipoprotein A-IMilano/1-Palmitoyl-2-Oleoyl) Tj ETQqO American College of Cardiology, 2008, 51, 1098-1103.	0 0 rgBT 2.8	Overlock 10 87
5	Glycoconjugates of gadolinium complexes for MRI applications. Chemical Communications, 2006, , 1064.	4.1	84
6	Ocular Surface Injury Induces Inflammation in the Brain: In Vivo and Ex Vivo Evidence of a Corneal–Trigeminal Axis. , 2014, 55, 6289.		44
7	Neural Stem Cells of the Subventricular Zone Contribute to Neuroprotection of the Corpus Callosum after Cuprizone-Induced Demyelination. Journal of Neuroscience, 2019, 39, 5481-5492.	3.6	42
8	Evidence for <i>in vivo</i> macrophage mediated tumor uptake of paramagnetic/fluorescent liposomes. NMR in Biomedicine, 2009, 22, 1084-1092.	2.8	36
9	Multispectral MRI with Dual Fluorinated Probes to Track Mononuclear Cell Activity in Mice. Radiology, 2019, 291, 351-357.	7.3	36
10	Growth Defects and Impaired Cognitive–Behavioral Abilities in Mice with Knockout for Eif4h, a Gene Located in the Mouse Homolog of the Williams-Beuren Syndrome Critical Region. American Journal of Pathology, 2012, 180, 1121-1135.	3.8	35
11	MR Imaging of Brachial Plexus and Limb-Girdle Muscles in Patients with Amyotrophic Lateral Sclerosis. Radiology, 2016, 279, 553-561.	7.3	32
12	Targeted inducible delivery of immunoactivating cytokines reprograms glioblastoma microenvironment and inhibits growth in mouse models. Science Translational Medicine, 2022, 14, .	12.4	32
13	A <i>R</i> _{2p} / <i>R</i> _{1p} Ratiometric Procedure to Assess Matrix Metalloproteinaseâ€2 Activity by Magnetic Resonance Imaging. Angewandte Chemie - International Edition, 2013, 52, 3926-3930.	13.8	30
14	A Bioorthogonal Probe for Multiscale Imaging by ¹⁹ F-MRI and Raman Microscopy: From Whole Body to Single Cells. Journal of the American Chemical Society, 2021, 143, 12253-12260.	13.7	29
15	Down-sizing of neuronal network activity and density of presynaptic terminals by pathological acidosis are efficiently prevented by Diminazene Aceturate. Brain, Behavior, and Immunity, 2015, 45, 263-276.	4.1	27
16	Novel Gd(III)â€based probes for MR molecular imaging of matrix metalloproteinases. Contrast Media and Molecular Imaging, 2012, 7, 175-184.	0.8	23
17	Novel MRI and fluorescent probes responsive to the Factor XIII transglutaminase activity. Contrast Media and Molecular Imaging, 2010, 5, 213-222.	0.8	22
18	Design of fluorinated hyperbranched polyether copolymers for ¹⁹ F MRI nanotheranostics. Polymer Chemistry, 2020, 11, 3951-3963.	3.9	22

LINDA CHAABANE

#	Article	IF	CITATIONS
19	Biomimetic MRI Contrast Agent for Imaging of Inflammation in Atherosclerotic Plaque of ApoEâ^'/â^' Mice. Investigative Radiology, 2009, 44, 151-158.	6.2	20
20	Quantification of multicontrast vascular MR images with NLSnake, an active contour model: In vitro validation and in vivo evaluation. Magnetic Resonance in Medicine, 2004, 51, 370-379.	3.0	19
21	Defining Peripheral Nervous System Dysfunction in the SOD-1 ^{G93A} Transgenic Rat Model of Amyotrophic Lateral Sclerosis. Journal of Neuropathology and Experimental Neurology, 2014, 73, 658-670.	1.7	18
22	In Vivo Magnetic Resonance Imaging of Large Spontaneous Aortic Aneurysms in Old Apolipoprotein E-Deficient Mice. Investigative Radiology, 2004, 39, 585-590.	6.2	15
23	Tumor microvasculature observed using different contrast agents: a comparison between Gd-DTPA-Albumin and B-22956/1 in an experimental model of mammary carcinoma. Magnetic Resonance Materials in Physics, Biology, and Medicine, 2008, 21, 169-176.	2.0	15
24	Skeletal Muscle Proteomic Profile Revealed Gender-Related Metabolic Responses in a Diet-Induced Obesity Animal Model. International Journal of Molecular Sciences, 2021, 22, 4680.	4.1	15
25	Nonâ€invasive visual evoked potentials to assess optic nerve involvement in the dark agouti rat model of experimental autoimmune encephalomyelitis induced by myelin oligodendrocyte glycoprotein. Brain Pathology, 2020, 30, 137-150.	4.1	14
26	Fluorinated PLGA Nanoparticles for Enhanced Drug Encapsulation and ¹⁹ Fâ€NMR Detection. Chemistry - A European Journal, 2020, 26, 10057-10063.	3.3	14
27	JAB1 deletion in oligodendrocytes causes senescence-induced inflammation and neurodegeneration in mice. Journal of Clinical Investigation, 2022, 132, .	8.2	12
28	In vivo magnetic resonance spectroscopy in the brain of <i>Cdkl5</i> null mice reveals a metabolic profile indicative of mitochondrial dysfunctions. Journal of Neurochemistry, 2021, 157, 1253-1269.	3.9	10
29	High-Resolution Magnetic Resonance Imaging at 2 Tesla: Potential for Atherosclerotic Lesions Exploration in the Apolipoprotein E Knockout Mouse. Investigative Radiology, 2003, 38, 532-538.	6.2	9
30	The Danger Signal Extracellular ATP Is Involved in the Immunomediated Damage of α-Sarcoglycan–Deficient Muscular Dystrophy. American Journal of Pathology, 2019, 189, 354-369.	3.8	9
31	Microimaging of atherosclerotic plaque in animal models. Magnetic Resonance Materials in Physics, Biology, and Medicine, 2000, 11, 58-60.	2.0	7
32	Optic nerve involvement in experimental autoimmune encephalomyelitis to homologous spinal cord homogenate immunization in the dark agouti rat. Journal of Neuroimmunology, 2018, 325, 1-9.	2.3	6
33	A Hypothalamic-Controlled Neural Reflex Promotes Corneal Inflammation. , 2021, 62, 21.		5
34	Title is missing!. Investigative Radiology, 2003, 38, 532-538.	6.2	4
35	Microimaging of atherosclerotic plaque in animal models. Magnetic Resonance Materials in Physics, Biology, and Medicine, 2000, 11, 58-60.	2.0	3
36	Dynamic Active Contour Model for Size Independent Blood Vessel Lumen Segmentation and Quantification in High-Resolution Magnetic Resonance Images. Lecture Notes in Computer Science, 2001, , 264-273.	1.3	3

LINDA CHAABANE

#	Article	IF	CITATIONS
37	Hydrophobinâ€Coated Solid Fluorinated Nanoparticles for ¹⁹ Fâ€MRI. Advanced Materials Interfaces, 0, , 2101677.	3.7	3
38	MRI and PET Compatible Bed for Direct Co-Registration in Small Animals. IEEE Transactions on Nuclear Science, 2013, 60, 1596-1602.	2.0	2
39	Evaluation of the co-registration capabilities of a MRI/PET compatible bed in an Experimental autoimmune encephalomyelitis (EAE) model. Nuclear Instruments and Methods in Physics Research, Section A: Accelerators, Spectrometers, Detectors and Associated Equipment, 2013, 702, 108-110.	1.6	2
40	Doseâ€dependent effect of myelin oligodendrocyte glycoprotein on visual function and optic nerve damage in experimental autoimmune encephalomyelitis. Journal of Neuroscience Research, 2022, 100, 855-868.	2.9	1
41	Persistent acidosis affects electrophysiological transmission and synaptic homeostasis of neuronal networks. Journal of Neuroimmunology, 2014, 275, 146-147.	2.3	0
42	Role of endogenous neural precursor cells in demyelination and remyelination after cuprizone-induced injury. Journal of Neuroimmunology, 2014, 275, 188-189.	2.3	0
43	Fingolimod may support neuroprotection via blockade of astrocyte S1P and cytokine signaling cascades in Multiple Sclerosis. Journal of Neuroimmunology, 2014, 275, 144-145.	2.3	0